American Mineralogist, Volume 83, pages 918–924, 1998

Characterization of carbon compounds on a pyroxene surface from a gabbro xenolith in basalt by time-of-flight secondary ion mass spectrometry

E.A. MATHEZ[1,*] AND D.M. MOGK[2]

[1]Department of Earth and Planetary Sciences, American Museum of Natural History, New York, New York 10024, U.S.A.
[2]Department of Earth Sciences, Montana State University, Bozeman, Montana 59717, U.S.A.

ABSTRACT

Time-of-flight secondary ion mass spectrometry (TOF-SIMS) yields mass spectra of the upper several monolayers of an analytical surface. The applicability of TOF-SIMS to the characterization of C compounds on crack surfaces in rocks is demonstrated. A pyroxene grain recovered from the interior of a gabbro xenolith from the 1801 flow of Haulalai volcano, Hawaii, was chosen for this initial study because well-developed carbonaceous films are known to exist on many of the crack surfaces in these rocks. In addition to the anticipated major elements (Si, Al, Fe, Mg, Ca), several minor and trace elements (B, Li, Na, Ti, Mn, Co, Ni, Cu) were identified in the positive ion mass spectra. The unsputtered surface is covered with a hydrocarbon-rich layer, as indicated by the presence of numerous light C_xH_y fragments as well as several masses of several hundred atomic mass units (amu). This layer is much better developed than the ubiquitous atmosphere-derived hydrocarbon layer observed on nominally clean, unsputtered surfaces and therefore must be indigenous. High concentrations of Ni and Cu are associated with the C-rich layer and may exist as organo-metallic compounds. Several C-N fragments, possibly indicative of biogenic compounds, were also identified in negative ion spectra. Imaging reveals the presence of localized islands enriched in oxides of Si, Al, Na, and Ca beneath the carbonaceous layer. This study demonstrates that TOF-SIMS can be used to provide unique and geochemically useful information on crack surfaces in rocks.

INTRODUCTION

Analysis of crystalline rocks using surface-sensitive spectroscopies reveals that C is ubiquitous as a thin film on microcrack surfaces (e.g., Tingle et al. 1991). The origin of the carbonaceous films is not obvious; one hypothesis, proposed for peridotite xenoliths in basalts, is that they form rapidly by reaction of the fresh mineral surface with whatever fluid or gas penetrates the crack initially (Mathez 1987). Such carbonaceous films could well be relegated to the status of mere curiosities except that they may influence electrical conductivity of rocks (Shankland et al. 1997), participate in trace element partitioning and redox reactions, and represent evidence of, or provide sustenance for, a subsurface biological community.

A major obstacle to deducing how carbonaceous films form is the few means available for chemical and spatial characterization. Electron microprobe techniques have proven useful for determining the distribution of C-bearing microcracks but provide little information about composition; analysis by Auger spectroscopy (AES) is hampered by problems associated with working with insulators and does not provide chemical information; and X-ray photoelectron spectroscopy (XPS) has been used to detect hydrocarbons on crack surfaces and infer information on the chemical state of C (Mathez 1987), but identification of specific molecular species is beyond the capability of this technique.

The purpose of this communication is to report on the applicability of time-of-flight secondary ion mass spectrometry (TOF-SIMS) to the characterization of C in rocks. In our development of the methodology, it has become clear that TOF-SIMS holds great promise for determining the composition and distribution of C compounds, including organics, and more generally for studies that require detection and identification of contaminants in microcracks in rocks.

ANALYSIS

Description of technique

TOF-SIMS is a surface-sensitive technique capable of providing high-resolution mass spectra (0.0001 amu) over a mass range of 1 to 10 000 amu, and maps of the distribution of individual masses with submicron spatial resolution. Such analysis obviously entails minimal damage of the analytical surface by the incident ion beam. This is in contrast to the more routinely used dynamic SIMS (ion probe), in which elemental sensitivity is maximized by dissociating ions from within a volume of the sample by sputtering. Detailed descriptions of TOF-SIMS may

* E-mail:mathez@amnh.org

be found in Brown et al. (1990) and Benninghoven (1994).

The bombardment of a surface with primary ions creates a collision cascade of atoms within the target. The collision cascade may reach the surface. When it does so near the impact site of the primary ion, the atoms near the end of the collision cascade generally still possess high elastic energies. The result is that large surface molecules are fragmented, and the ions ejected from the surface are atomic species (e.g., O^-) or tightly bonded ion clusters (e.g., CN^-). This process is known as ''prompt collisional sputtering.'' Atomic-collision cascades that reach the surface remote from the impact site possess lower elastic energies. Thus larger ion clusters or even molecular ions tend to be preserved during ejection in the process of ''slow collisional sputtering.'' Collision cascades that migrate to the surface yet further from the impact site may have just enough energies to desorb, but not destroy, large polymer fragments.

This leads to the concept of the ''static limit,'' which is defined as the primary ion dose at which modification of the analytical surface is not observable in the secondary ion spectrum. The static limit is normally taken to be 10^{12} to 10^{13} ion/cm^2. A primary ion dose of 10^{12} ion/cm^2 nominally consumes $\approx$0.1% of the top monolayer, so the secondary spectrum does not change during prolonged analysis. Analysis under conditions of primary beam current density below the static limit is known as ''static SIMS'' and is the desired mode of operation in TOF-SIMS, especially when the goal is to identify polymers. In dynamic SIMS, on the other hand, the entire surface is sputtered away with the use of much higher primary beam currents. The characteristics and class of problems to which TOF-SIMS and dynamic SIMS are applicable are thus much different.

In the present experiments a Ga liquid-metal primary beam source was used. The advantage of liquid metal sources is that they are sufficiently bright to yield analytically useful beam currents in beams having diameters as small as 50 nm, which is desirable for imaging. In addition, surface bombardment by heavy particles at energies of 10 to 20 KeV maximizes secondary ion yield. The timing necessary for mass spectrometry by time-of-flight is provided by pulsing of the primary beam. The important features of the time-of-flight mass spectrometers are that secondary ions are detected quasi-simultaneously, the relationship between mass and flight time is valid over a wide mass range, and the transmission, sensitivity, and mass resolution are high compared to mass spectrometers in which mass scans are necessary. The high spatial resolution of the primary beam and transmission of the spectrometer combine to allow for a complete mass spectrum to be acquired for every pixel in an imaging mode.

An important feature of TOF-SIMS is its monolayer sensitivity. Such an analytical depth resolution is shallower than in electron spectroscopy, in which resolution is typically several nanometers. On the other hand, several factors, including atomic mass, solid-state bonding, electronic state of the material being analyzed, and primary beam current density, strongly influence the secondary ion yield such that yields of ions having identical concentrations may vary by orders of magnitude. The fact that TOF-SIMS is surface sensitive is precisely the reason it is difficult to quantify. In a bulk analysis, it is possible to calibrate the collective ''matrix effects'' by comparison of an unknown with a standard of similar composition, as is routinely done in quantification of dynamic SIMS. But in a surface analysis, both the bulk and the surface must be matched in a standard. It is emphasized that mass intensity is not a good indication of mass concentration and that TOF-SIMS data are typically qualitative.

TOF-SIMS has proven to be a powerful means of identifying large surface organic molecules (e.g., Hercules 1993). It has found use, for example, in characterization of polymers, adhesion studies, failure analysis, semiconductor research, evaluation of medical delivery devices, analysis of paper and inks, and even detection of chemical warfare agents on natural materials. Geologically relevant studies on the detection of contaminants on mineral and other natural surfaces (Groenewold et al. 1995a, 1995b, 1995c, 1996; Ingram et al. 1997) demonstrate the great potential of TOF-SIMS to classes of problems involving adsorption, heterogeneous catalysis, diffusion, and precipitation/dissolution processes. Other relevant studies have been conducted on coal (Hou et al. 1995; Buckley and Lamb 1996), interplanetary dust particles (Stephan et al. 1994), and calcite (Stipp et al. 1997); these further illustrate the power of the technique in the imaging of surface compounds.

TOF-SIMS analysis of rocks

The instrument used in the present study is a PHI-Evans T-2000 of the Image and Chemical Analysis Laboratory at Montana State University. The primary beam was ^{69}Ga operated at 15 KeV with a sample bias of $\pm$3 KeV, depending on whether positive or negative secondary ions were being collected. The primary beam current was $\approx$1.5 na and the beam diameter 0.5 μm. The post acceleration voltage was set at 2 keV for most analyses. Rocks are insulators, so their analysis by charged particles is always more complicated than analysis of conductive materials. No difficulties were experienced during data collection when a stainless steel grid was placed over and in contact with the analytical surface.

Two types of analyses were carried out. Ion imaging of the surface was conducted by rastering the primary beam over the surface. During this analysis, the instrument was operated in the ''bunched'' mode, which maximizes spatial resolution but limits mass resolution to only $\approx$1000. Ion spectra were also collected in a high mass resolution mode to allow specific identification of certain masses. In both cases, both positive and negative secondary ion spectra were collected because it was found that they contained substantially different information. In the interpretation of the spectra, we found it

useful to identify peaks from low to high mass rather than adopting the more orthodox approach of identifying the high-mass peaks first. This procedure was dictated by the fact that natural surfaces are complex and the guidelines for interpretation that would normally accompany surfaces produced in controlled experiments were absent.

Several problems are specific to the analysis of fracture surfaces in rocks. To preserve petrographic context, it was found useful to produce polished faces of free-standing rock fragments (i.e., those not mounted on glass and thus unexposed to substances such as epoxy) and examine microcracks intersecting the polished surface at low angles. The limitation is that cracks cannot be too deep or else no signal can be extracted from them, probably because the local topography causes too great a distortion in the local electronic field. An additional potential problem is that polished samples are obviously exposed to the polishing media, in the present case, water-alumina slurries. No obvious contaminants from such treatment have been identified on the crack surfaces.

In some cases, it is possible to recover quasi-flat microcrack surfaces. The advantage of analyzing such surfaces is that they are pristine, being exposed only to air during a short interval of time between crushing of the rock and introduction of a fragment into the vacuum chamber. The disadvantage is that mass resolution may be slightly degraded because surface topographic variations cause slight variations in focus of the secondary ion beam. Finally, even virgin surfaces exposed only to air are always covered with atmospheric contaminants. Contaminants were removed by sputtering with high-current bursts of Ga^+ alternating with a flood of electrons (for charge compensation) at 2 s intervals. Sputtering obviously removes the original surface but may also modify the structure of the newly exposed one. For most experiments, spectra were acquired both before and after sputtering. Contaminants could be clearly identified when they rested on the polished, nominally clean surfaces.

Observations of carbon in rocks

Several different samples have been studied with TOF-SIMS. Among these is an olivine gabbro xenolith from the Hualalai 1801 flow, Hawaii (AMNH sample HL89-1). This sample was chosen as the focus of this report because it provides both new information on C compounds and illustrates the applicability of TOF-SIMS to the study of crack surfaces. It was initially chosen for examination because the C in other xenoliths from the same locality has been studied in detail. Well-developed carbonaceous films exist on many fracture surfaces in these rocks. These films are clearly and easily distinguished from the several monolayers of carbonaceous contaminant present on practically all surfaces exposed to the atmosphere. For example, carbon maps produced with the electron probe (e.g., Mathez 1987) show no detectable C on polished surfaces but significant amounts on crack surfaces. Using XPS Mathez (1987) found that the C_{1s} photoelectron spectra generated from pyroxene microfracture surfaces were reasonably reproducible from location to location, and could be deconvoluted to represent four peaks with identical spectral shapes and separation distances, which was interpreted to indicate the presence of C in four different functional groups.

The sample for TOF-SIMS was recovered by crushing of the rock. The fragment chosen for analysis is a blocky pyroxene grain with a quasi-flat fracture surface. It was recovered from the interior of the xenolith, and care was taken that the analytical surface did not make contact with any objects or fluids during recovery.

Mass spectra

Positive and negative mass spectra have been generated for a 60×60 μm unsputtered and sputtered region on the pyroxene fracture surface. It is emphasized that the film on this surface is not dominantly atmospheric contamination. The spectral signals of C-bearing fragments from the unsputtered surface are much more intense than those from unsputtered polished or even crack surfaces of other samples exposed to the atmosphere, and the sputtering induced a dramatic change in the composition of the pyroxene surface not observed for other samples. In addition, the pyroxene surface was sputtered for 4 min, a procedure that nominally removed about 40 nm of the surface; yet small amounts of C were still evident on it. Films of such thicknesses are consistent with our ability to detect them with the electron probe.

The clearly identified species in the mass spectra are listed in Table 1. The *m/z* peak at 1 (H) is prominent but decreases in abundance with sputtering (Figs. 1a and 1b). Peaks at 6 (Li) and 11 (B) are present in the unsputtered spectrum; with sputtering, the Li peak was enhanced and B peak disappeared (Table 1). SIMS is highly sensitive to Li, and we commonly observed Li in the spectra from other samples. Peaks at *m/z* 12, 13, 14, and 15 (Fig. 1a) may be rationally fit to C and the fragments CH, CH_2, and CH_3, respectively. The ratio of C:($CH+CH_2+CH_3$) increases from 0.33 to 0.56 with sputtering, probably due to loss of the parent molecules.

In the *m/z* range 20 to 30 (Figs. 1a–1d), the prominent peaks represent the ions Na, Mg, Al, and Si and their less abundant isotopes (^{25}Mg, ^{26}Mg, ^{29}Si, and ^{30}Si). Metal hydride peaks (e.g., HMg) are also present. These are unresolved from the primary elemental peaks, and their presence is deduced by the fact that the relative peak heights are not consistent with isotopic abundance. Various C-H fragments are also present and clearly resolvable at the shoulders of the metal ion peaks in the unsputtered spectrum. For example, C_2H_2, H_2Mg, and ^{26}Mg are all nominally at mass 26, but two peaks—one from C_2H_2 and the other from $H_2Mg + {}^{26}Mg$—are clearly resolvable. Again, the intensities of the peaks due to C-H fragments are much diminished by sputtering (Table 1). The relative metal ion abundances also change dramatically with sputtering (e.g., Al vs. $H_2Mg + {}^{26}Mg$).

Throughout the *m/z* range 37 to 65, several uniquely identifiable C-H fragments are present on the unsputtered

TABLE 1. Selected peaks in the mass spectra from an unsputtered and sputtered pyroxene microfracture surface, sample HL89-1

Mass	Species	Intensity, unsputtered	Intensity, sputtered*
	Positive spectra		
1	H	1.793	0.660
7	Li	0.003	0.022
11	B	0.007	—†
12	C	0.292	0.093
13	CH	0.202	0.048
14	CH_2	0.219	0.057
15	CH_3	0.475	0.061
16	O		0.060
20	HF		0.008
23	Na	5.11	1.54
24	Mg	2.50	24.0
25	^{25}Mg + HMg	0.619	4.51
26	^{26}Mg + H_2Mg	0.423	4.10
26	C_2H_2	0.302	
27	Al	10.9	3.96
27	C_2H_3	1.87	0.146
28	Si	1.97	0.670
28	C_2H_4	0.364	0.018
29	^{29}Si + HSi	1.06	0.097
29	C_2H_5	1.03	0.102
30	^{30}Si + H_2Si	0.118	0.026
30	C_2H_6	0.115	0.018
31	CH_3O	0.093	—
37	C_3H	0.027	0.006
38	C_3H_2	0.101	—
39	K	0.395	0.059
39	C_3H_3	0.910	0.128
40	Ca	1.45	1.17
40	C_3H_4	0.171	—
41	HCa	—	0.437
41	C_3H_5	1.68‡	0.152
42	H_2Ca	—	0.076
42	C_3H_6	0.297§	0.020
43	N_3H + C_2H_3O	0.536	—
43	C_3H_7	0.854	0.128
44	C_3H_8 + ^{44}Ca + OSi	0.083	0.059
48	Ti		0.058
49	HTi + ^{49}Ti		0.016
50	C_4H_2	0.051	—
51	C_4H_3	0.118	—
52	C_4H_4	0.055	—
53	C_4H_5	0.278	0.020
54	^{54}Fe	0.668	2.12
54	C_4H_6	0.090	—
55	Mn	0.859	0.651
55	C_4H_7	0.794	0.059
56	Fe + CaO	10.5	26.8
56	C_4H_8	0.101	—
57	HFe + ^{57}Fe + HCaO	3.33	3.10
57	C_4H_9	0.371	0.039
58	Ni	5.10	0.483
59	Co + HNi	0.580	0.052
60	^{60}Ni	2.01	—
61	^{61}Ni + ?	0.192	—
62	^{62}Ni	0.266	—
63	Cu	11.48	0.264
64	^{64}Ni + ?	0.185	—
65	^{65}Cu + ?	5.26	0.153
	Negative spectra		
1	H	19.7	7.58
12	C	3.87	1.04
13	CH	7.22	2.19
14	CH_2	1.03	0.329
15	HN		0.011
15	CH_3	0.025‖	0.079
16	O	18.5	16.5
17	OH	12.9	14.9
18	H_2O	0.101	0.182
19	F	0.473	0.890
24	C_2	1.03	0.519
25	C_2H	2.48	1.56
26	CN	1.81	4.40
27	C_2H_3	0.052	0.076
29	CHO	0.073	0.015
30	NO	0.026	0.012
31	CH_3O	0.029	0.017
32	O_2	0.557#	1.00
32	S		0.218
33	HO_2	0.167**	1.05
33	HS		0.039
35	Cl	2.70	4.53
37	^{37}Cl	0.859	1.57
37	C_3H	—	0.085
40	C_2O	—	0.101
41	C_2HO	—	0.206
42	CNO	0.291	1.25
45	CHO_2	—	1.23
48	C_4	—	0.042
49	C_4H	—	0.158

Note: Intensities are given as counts as a percent of total counts.
* Excludes Ga, which becomes part of the surface by implantation.
† Undetected at the 0.001% level or the species is not a good fit.
‡ Probably unresolved with HCa.
§ Probably unresolved with H_2Ca.
‖ Unresolved with HN.
Unresolved with S.
** Unresolved with HS.

surface but generally absent from the sputtered one (Figs. 1e and 1f). In a group of fragments with the same number of C, those with an odd number of H are relatively more abundant than those with the immediately lower even number, reflecting the greater stability of ions containing paired than unpaired electrons in the C-H bonds (e.g., C_3H_3 and C_3H_5 vs. C_3H_2 and C_3H_4, Table 1). The C-H peaks generally fall on the shoulders of peaks of metal ion fragments. Although those from the dissociated ions K, Ca, Ti, Fe, etc. are readily identifiable, numerous other fragments are present in this mass range and, at least in these spectra, cannot be identified uniquely. Among these is CaO (mass 56), which represents a significant (but recognized) interference with ^{56}Fe. Both Ni (masses 58, 60, 61, 62, 64) and Cu (masses 63 and 65) are present on the unsputtered surface, but on the sputtered surface Ni appears to be absent completely and Cu is much less abundant (Figs. 1a and 1b). These elements have been observed in X-ray spectra of Hualalai carbon (Mathez 1987) and, since they disappeared along with the hydrocarbons with sputtering, they may exist as organometallic compounds. They have not been observed on crack surfaces in other rocks.

Most peaks in positive mass spectra below about *m/z* 70 can be uniquely identified by the usual criteria, namely that intensities are dictated by relative isotopic abundance and composition and that the different masses are rationally consistent with each other. Identification of masses greater than 70 becomes progressively more uncertain, however, so we resist making specific assignments. There

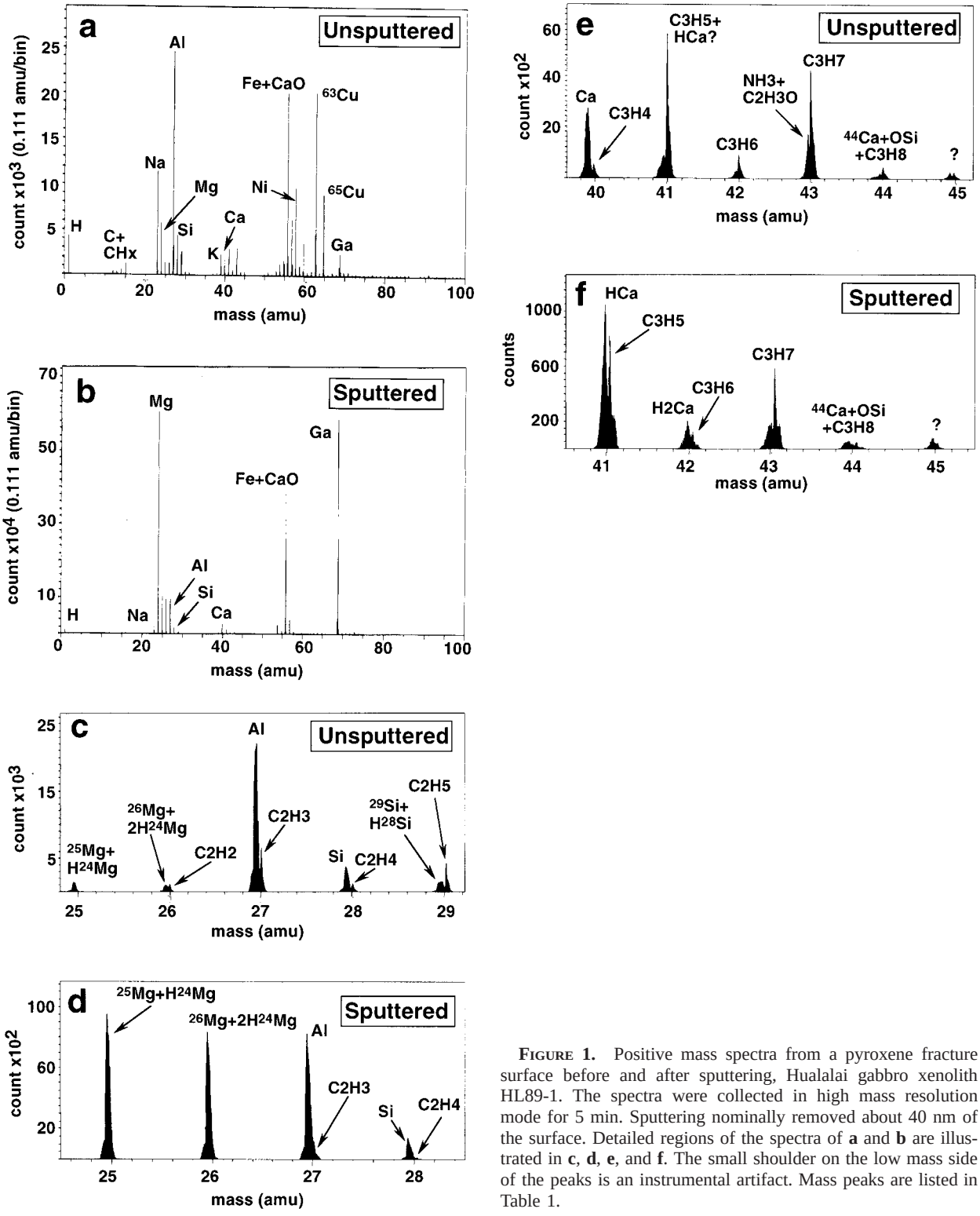

Figure 1. Positive mass spectra from a pyroxene fracture surface before and after sputtering, Hualalai gabbro xenolith HL89-1. The spectra were collected in high mass resolution mode for 5 min. Sputtering nominally removed about 40 nm of the surface. Detailed regions of the spectra of **a** and **b** are illustrated in **c**, **d**, **e**, and **f**. The small shoulder on the low mass side of the peaks is an instrumental artifact. Mass peaks are listed in Table 1.

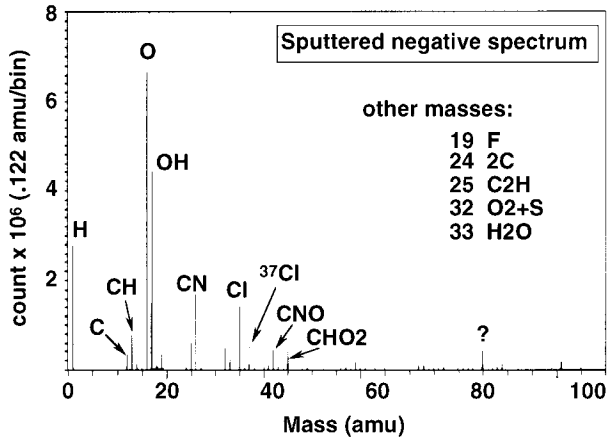

FIGURE 2. Negative mass spectrum corresponding to the positive spectra of Figure 1. Note that this is from the sputtered surface. The spectrum was collected for 30 min. Mass peaks are listed in Table. 1

are numerous low-intensity peaks in the range 70 to 110 in the spectrum of the unsputtered surface that disappeared upon sputtering. In contrast, certain peaks and groups of peaks emerged with sputtering, in particular those at *m/z* 80, 87, and 112. These are probably inorganic fragments from the mineral substrate, and there are typically several such fragments that fit the observed peaks. The spectrum of the unsputtered surface also contains a set of peaks in the range 440 to 500, the most prominent of which are *m/z* 440, 454, 480, 481, 482, 494, 495, and 496. These peaks must be from hydrocarbons because they are absent on the sputtered surface and have not been observed in mass spectra from other samples.

Major peaks in the negative spectra (Fig. 2, Table 1) are at *m/z* 1 (H), 16 (O), and 17 (OH). Peaks of much lower intensity at *m/z* 12, 13, 14, and 15 correspond to C and various CH fragments. In the sputtered surface spectrum, HN can be distinguished from CH_3 and these peaks are unresolved in the spectrum from the unsputtered surface. Fluorine is present in both spectra. When *m/z* peaks at 24, 25, and 26 are assigned to C_2, C_2H, and CN, excellent fits are obtained by the assignment of the two peaks at *m/z* 32 to O_2 and S, of the peaks at *m/z* 35 and 37 to Cl, and of the peak at *m/z* 42 to CNO. Additional evidence for the existence of C-N fragments are the presence of small but resolvable peaks representing C_2N and C_2NH at the shoulders of larger peaks representing C_3H_2 and C_3H_3 (*m/z* 38 and 39). These various C-N fragments are consistent with the possibility that some (or all) of the carbon compounds are biogenic, but they do not demand this interpretation. The C-N compounds are less abundant on the unsputtered than sputtered surface (Table 1), indicating that they persist below the carbonaceous layer.

The spectrum of the sputtered surface also contains C_x and C_xH fragments, e.g., C_4 and C_4H_2 at *m/z* 48 and 50. Peaks above about *m/z* 50 cannot be identified uniquely,

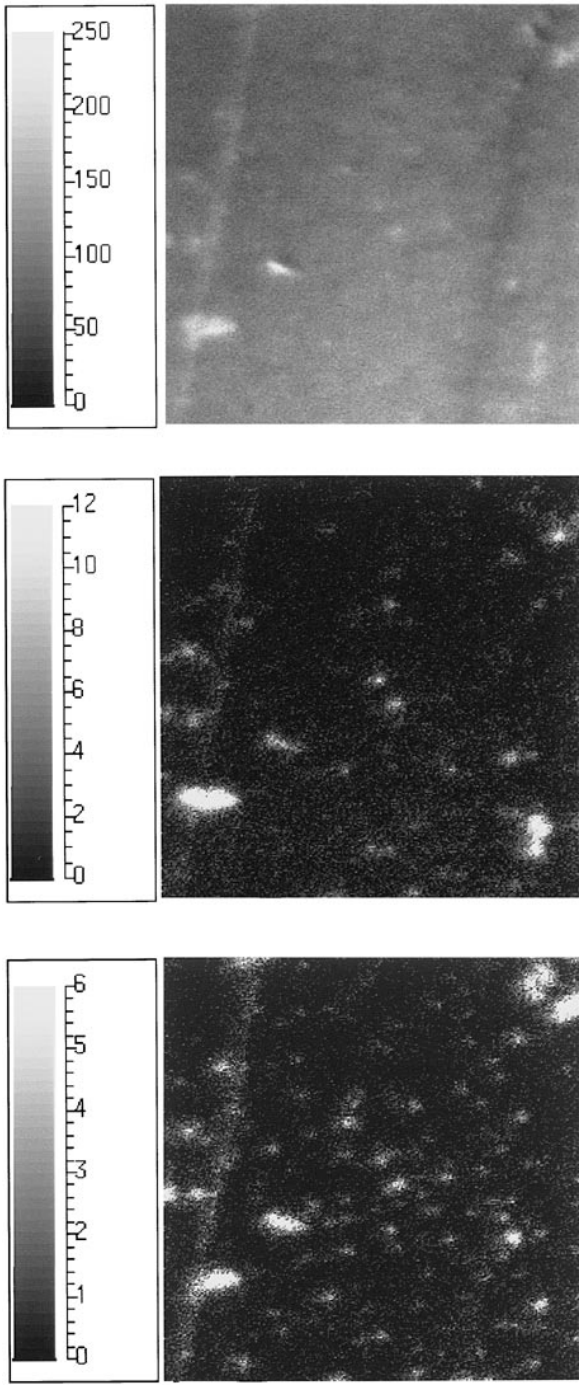

FIGURE 3. The total positive ion (top), Na (middle), and Si (bottom) images of the sputtered, analyzed pyroxene fracture surface. The images are 60 μm on a side. The spectra of Figure 1 are of this area. The total collection time was 10 min. Despite this being a relatively clean pyroxene surface, the peak from Si is not intense, as can be seen from Figure 1b.

but they are consistent with various COH, COHS, and COCl fragments. Several heavy masses, in particular at *m/z* 85, 88, and 101, are present on the sputtered surface but not on the unsputtered one. They are also present in spectra from our other samples. Several plausible inorganic fragments correspond to each of these masses (e.g., HSiFe at *m/z* 85). As in the positive ion spectrum, several heavy masses are found in the unsputtered negative spectrum, mostly in the *m/z* range 260–340. These have not been observed in other samples and are probably hydrocarbons.

Ion images

The distribution of individual masses was also determined on the analytical surface. Images 60 μm on a side were found to be most useful for the present purposes. Images of the unsputtered surface for the prominent masses in the spectra of Figure 1 exhibit no obvious features. The map of the sputtered surface for total positive ions (Fig. 3a) reveals two parallel, linear features, which are interpreted to be pyroxene cleavage planes intersecting the analytical surface. An array of islands enriched in Na, Al, Si, and Ca (*m/z* 23, 27, 28, and 40, respectively) also emerged (Figs. 3b and 3c). There are no correspondingly enriched masses in the negative spectrum, so the islands are probably composed of an oxygen-based compound. The islands are beneath the carbonaceous layer and thus may have formed first. We interpret them to represent a leached surface layer formed by reaction of the mineral with either volcanic gas or acid waters.

Conclusion

TOF-SIMS is a potentially powerful tool for the study of surfaces in rocks and provides new opportunities to identify and map molecular compounds that are otherwise not resolvable using other microbeam techniques. High mass and spatial resolution, both laterally and in depth, combine to yield compositional and spatial information that is unique and specific enough to be of utility in a geochemical context. The natural surfaces do present certain challenges. Primary among these is their chemical complexity, which renders the mass spectra themselves complex and limits their interpretation. The problem of interpretation should be less severe in spectra from controlled experiments or analyses in which specific masses are sought.

TOF-SIMS has allowed us to recognize a complex inventory of molecular species, transparent to other spectroscopies, on a microcrack in a pyroxene. These species appear to represent fragments of heavier hydrocarbons and include C-N and possibly organometallic compounds. These compounds are probably present in many different rocks, and they may be involved in a variety of biogeochemical processes as well.

Acknowledgments

We thank the cast of characters, especially Nancy Equall and Recep Avci, of the Imaging and Chemical Analysis Laboratory, Montana State University, for their help and patience and three reviewers, whose efforts served to improve this paper. This work was supported by a grant to EAM from the Geosciences Research Program, Office of Basic Energy Sciences of the Department of Energy.

References cited

Benninghoven, A. (1994) Surface analysis by secondary ion mass spectrometry. Surface Science, 299/300, 246–260.

Brown, A.W., Vickerman, J.C., and Reed, N.M. (1990) Secondary ion mass spectrometry: principles and applications, 360 p. Oxford University Press, New York.

Buckley, A.N. and Lamb, R.N. (1996) Surface chemical analysis in coal preparation research: complementary information from XPS and TOF-SIMS. International Journal of Coal Geology, 32, 87–106.

Groenewold, G.S., Ingram, J.C., Delmore, J.E., and Appelhans, A.D. (1995a) Static secondary ionization mass spectrometry analysis of tributyl phosphate on mineral surfaces. Effect of Fe (II). Journal of the American Society of Mass Spectrometry, 6, 165–174.

Groenewold, G.S., Ingram, J.C., Delmore, J.E., Appelhans, A.D., and Dahl, D. (1995b) Rapid dectection of tri-n-butul phosphate on environmental surfaces using static SIMS. Journal of Hazardous Materials, 41, 359–370.

———(1995c) Detection of 2-chloroethyl ethyl sulfide and sulfonium ion degradation products on environmental surfaces using static SIMS. Environmental Science and Technology, 29, 2107–2111.

Groenewold, G.S., Ingram, J.C., Gianotto, A.K., Appelhans, A.D., and Delmore, J.E. (1996) Static secondary ionization mass spectrometry detection of cyclohexylamine on soil surfaces exposed to laboratory air. Journal of the American Society of Mass Spectrometry, 7, 168–172.

Hercules, D.M. (1993) Surface analysis of organic materials with TOF-SIMS. Journal of Molecular Structure, 292, 49–64.

Hou, X., Ren, D., Mao, H., Lei, J., Jin, K., Chu, P., Reich, F., and Wayne, D.H. (1995) Application of imaging TOF-SIMS to the study of some coal macerals. International Journal of Coal Geology, 27, 23–32.

Ingram, J.C., Groenewold, G.S., Appelhans, A.D., Delmore, J.E., Olson, J.E., and Miller, D.L. (1997) Direct surface analysis of pesticides on soil, leaves, grass, and stainless steel by static secondary ion mass spectroscopy. Environmental Science and Technology, 31, 402–408.

Mathez, E.A. (1987) Carbonaceous matter in mantle xenoliths: Composition and relevance to the isotopes. Geochimica et Cosmochimica Acta, 51, 2339–2347.

Shankland, T.J., Duba, A.G., Mathez, E.A., and Peach, C.L. (1997) Increase of electrical conductivity with pressure as an indicator of conduction through a solid phase in mid-crustal rocks. Journal of Geophysical Research, 102, 14,741–14,750.

Stephan, T., Jessberger, E.K., Klöck, W., Rulle, H., and Zehnpfenning, J. (1994) TOF-SIMS analysis of interplanetary dust. Earth and Planetary Science Letters, 128, 453–467.

Stipp, S.L.S, Kulik, A.J., Franzreb, K., Benoit, W., and Mathieu, H.J (1997) A combination of SFM and TOF-SIMS imaging for observing local inhomogenieties in morphology and composition: aged calcite surfaces. Surface and Interface Analysis, 25, 959–965.

Tingle, T.N., Mathez, E.A., and Hochella, M. (1991) Carbonaceous matter in peridotites and basalts studied by XPS, SALI and LEED. Geochimica et Cosmochimica Acta, 55, 1345–1352.

Manuscript received December 16, 1997
Manuscript accepted April 1, 1998
Paper handled by Robert F. Dymek